InN thin film lattice dynamics by grazing incidence inelastic x-ray scattering

J. Serrano,[1] A. Bosak,[2] M. Krisch,[2] F. J. Manjón,[3] A. H.

Romero,[4] N. Garro,[5] X. Wang,[6] A. Yoshikawa,[7] and M. Kuball[8]

[1]*ICREA - Departament de Física Aplicada,*

EPSC, Universitat Politècnica de Catalunya,

Carrer Esteve Terradas 5, E-08860 Castelldefels, Spain[*]

[2]*European Synchrotron Radiation Facility,*

B.P. 220, 38043 Grenoble cedex 9, France

[3]*Instituto de Diseño para la Fabricación y Producción Automatizada,*

MALTA Consolider Team, Universitat Politècnica de València,

Cno. de Vera s/n, 46022 València, Spain

[4]*CINVESTAV, Departamento de Materiales,*

Unidad Querétaro, Querétaro, Mexico 76230

[5]*Materials Science Institute, University of Valencia,*

PO Box 22085, E46071 Valencia, Spain

[6]*School of Physics, Peking University, Beijing 100871, China*

[7]*Graduate School of Electrical and Electronic Engineering,*

Chiba University 1-33 Yayoi-cho, Inage-ku, Chiba 263-8522, Japan

[8]*H. H. Wills Physics Laboratory, University of Bristol, Bristol BS8 1TL, United Kingdom*

(Dated: November 18, 2010)

Abstract

Achieving comprehensive information on thin film lattice dynamics has eluded so far well established spectroscopic techniques. This however is essential to gain insight into strain effects and to model heat transfer in advanced materials, often produced only as thin films. Indium nitride is an especially relevant example, due to the technological interest for optoelectronic and solar cell applications in combination of other group III-nitrides. We demonstrate here the novel application of grazing incidence inelastic x-ray scattering combined with *ab initio* calculations to determine the complete elastic stiffness tensor and the quasi-acoustic phonon dispersion relations of thin wurtzite indium nitride films.

Among the present technologically important semiconductors, indium nitride remains the least understood. The discovery of a 0.7 eV direct band gap of this material[1, 2] and its combination with other group-III nitrides is currently used for optoelectronic applications such as laser diodes and light-emitting diodes. The recent realization of p-type doping in InN[3, 4], commonly found more n-type, opened new possibilites for the achievement of high-efficient solar cells. Despite the intense research carried out on InN electronic and vibrational properties, there is a lack of experimental information on its phonon dispersion relations[5]. Usually grown by molecular beam epitaxy (MBE), state-of-the-art high quality InN films rarely exceed 10 micron thickness, thus preventing the use of standard bulk techniques to measure phonon dispersion relations. The available InN experimental data stem mainly from Raman and infrared spectroscopies[5, 6], and new technical developments are required to complete this information over the entire Brillouin zone (BZ).

Whereas large steps have been acomplished in the determination of lattice dynamics in single crystals, using both inelastic neutron (INS) and x-ray scattering (IXS) spectroscopies, there is a lack of corresponding techniques that can be employed for the study of thin films. In some cases bulk and surface lattice dynamics differ from each other[7] and it is essential to be able to probe both in the same experiment, and in many cases the material to be studied is only available as thin film such as InN. Since phonons mediate the heat transfer processes in semiconductors, thin film lattice dynamics play a fundamental role in modeling thermal device behavior in the quest for more effective opto- and microelectronic semiconductor devices[8].

In this letter, we demonstrate the potential of grazing incidence inelastic x-ray scattering to obtain information on the lattice dynamics of micrometer thick thin films. We also report here on the determination of the complete elastic stiffness tensor and the quasi-acoustic phonon dispersion relations of a 6.2μm InN film grown on GaN/sapphire.

The InN film studied of 2 micron thickness was deposited at 600 ^{0}C by MBE on a (0001) sapphire substrate using a 0.5μm GaN buffer layer. More details on the growth can be found in Ref.9. The film was unintentionally n-type doped, as common for InN, with a carrier concentration $n = 4 \times 10^{18}$ cm^{-3} and a mobility $\mu = 1420$ cm/Vs. Ω-scan x-ray diffraction experiments on the same sample yielded rocking curves of 0.09 and 0.22 degrees full-width-at-half-maximum (FWHM) for the 002 and 102 reflections, respectively, thus revealing an excellent single crystal quality. A rectangular shaped sample of 8×5

mm surface was employed in the IXS experiment. Figure 1(a) displays a scanning electron microscopy (SEM) image of the film section, showing the InN layer on top of the GaN buffer layer and the sapphire substrate.

Grazing incidence room temperature IXS experiments were performed in beam line ID28 at the European Synchrotron Radiation Facility, using an incident photon energy of 17.794 keV, as obtained from a Si 999 monochromator working in nearly backscattering geometry, and achieving 3 meV FWHM energy resolution. The beam was focused to a 60×250 μm^2 beam size (vertical×horizontal, FWHM) employing a cilindrical-toroidal mirror. A platinum-coated mirror was mounted along the beam path prior to the sample to make it impinge with a glancing angle of $\alpha_i =1.7$ degrees on the InN surface, as depicted in Fig. 1(b). This angle corresponds to an attenuation length of approximately 1.85 μm, which ensures probing phonons in the material and simultaneously avoiding spurious contributions from both the GaN buffer layer and the sapphire template. A similar setup had been successfully employed in the study of surface effects in Kohn anomalies in $NbSe_2$ 7 and in the investigation of surface acoustic dynamics of liquid indium[10].

Ab initio calculations of InN phonon dispersion relations and phonon eigenvectors were performed to ascertain the Brillouin zones suitable to achieve highest IXS intensity, according to the selection rules, and to analyze the experimental data. Calculations were based on Density Functional Theory as implemented within the ABINIT software package [11–13]. Both local density approximation (LDA) and generalized gradient approximations (GGA) were employed to ascertain the changes in the elastic stiffness tensor and the phonon dispersion relations with the exchange and correlation energy. Only the valence electrons were taken into account by using Troullier-Martins [14] and Hartwigsen-Goedecker-Hutter pseudopotentials [15] for LDA and GGA, respectively. A 60 Ha plane-wave energy cutoff was used within both LDA and GGA, combined with a $6 \times 6 \times 3$ k-point mesh for integration in order to ensure convergence of both total energy and stress tensor. The k-point grid was required to be increased further up to $14 \times 14 \times 8$ to converge better the elastic stiffness tensor. The ground state geometry was optimized relaxing both internal parameter and lattice constants at constant pressure upto a value of 3×10^{-2} GPa. The phonon frequencies and eigenvectors were calculated using a Fourier interpolation of a set of dynamical matrices calculated via non-linear response at a $6 \times 6 \times 3$ grid of q-points in the irreducible BZ.

Figure 2 shows a representative set of selected IXS spectra of transverse phonons along

the [010] direction of the BZ, i.e. Γ-M direction. The IXS signal is plotted as a function of momentum transfer q, with respect to the 200 Bragg peak. Beside the central elastic peak, a number of maxima appear at positive and negative energy transfers corresponding to phonon creation and annihilation processes, respectively. There is a sudden decrease in phonon intensity with increasing momentum transfer for the transverse acoustic modes (TA) due to the increase of excitation energy. The TA modes can be clearly distinguished from two higher energy dispersing excitations that stem from the E_2^{low} mode at $q = 0$. In this case, the E_2^{low} intensity is more strongly dependent on the change of phonon eigenvectors with momentum transfer. A Lorentzian function of 3 meV FWHM was used to fit the elastic peak, while similar functions with adjustable FWHM were convoluted to the elastic line to obtain the frequency of the phonon excitations.

Similar to Brillouin scattering, inelastic x-ray scattering allows one to probe the momentum transfer dependence of acoustic branches and hence derive the corresponding elastic stiffness constants. The advantage of using grazing incident IXS lies in the feasibility to obtain accurate information in thin films deposited on a substrate for nearly all directions of propagation, without the need to detach the film from the substrate. Grazing incidence IXS spectroscopy, in contrast to other techniques, is capable to choosing the probing depth in the film by varying the glancing angle. It therefore provides also a unique way to in addition investigate substrate-induced strain effects on the elastic constants even in submicron films.

In order to obtain the elastic constants, we first fitted the acoustic phonon branches at low q with a sinusoidal function $\omega(q) = A \sin(q\pi/B)$, where A and B are the fitting parameters. The limit for $q = 0$ of the slope of such function provides the sound velocity for the corresponding phonon branch. Table I displays the selected scattering geometries, polarization vectors and propagation directions, as well as the derived apparent sound velocities. These are in excellent agreement with those recently reported by Sarasamak *et al.*[16]. The sound velocity, V, is related to either a single or a combination of components of the elastic stiffness tensor via the Christoffels equation[17]. There are 5 independent components in the elastic stiffness tensor for the wurtzite structure: $C_{11} = \rho V(LA[100])^2$, $C_{33} = \rho V(LA[001])^2$, $C_{66} = \rho V(TA[010]_{\langle 100 \rangle})^2$, $C_{44} = \rho V(TA[100]_{\langle 001 \rangle})^2$, and C_{13}, where ρ is the mass density. Taking the experimental values for the lattice constants found in the IXS experiment, $a = 3.5340$Å and $c = 5.7088$Å, we employed a mass density $\rho = 6.93$ g/cm^3 for the derivation of the elastic constants. C$_{13}$ can only be obtained as a component in

the sound velocity along a direction neither in-plane nor aligned with the c-axis, and it was obtained by measuring the phonon energy of LA modes at small momentum transfer along the [2 0 3] direction and solving the Christoffels equation self-consistently.

Table II lists the elastic stiffness tensor obtained from the IXS data and compares them with results from our calculations and previously reported experimental[18] and *ab initio* calculated data[16, 19–21]. Note the large discrepancy between the values determined with IXS and those reported in Ref.18 from temperature dependente x-ray broadening in poly-crystalline InN. Our experimental values are in reasonable agreement with the calculations reported in Refs.16, 20, 21 and our own calculations. The use of LDA exchange and correlation term results in a significant improvement in the calculation of the axial elastic modulus, C_{33}, which stems from the longitudinal sound velocity propagating along the c-axis. The calculated value for C_{33} is particularly affected by the k-point grid employed, decreasing in value with increasing number of k-points. Our convergence tests ensure reliable results with a margin of 3 GPa for this elastic constant. Within this margin, the higher value obtained from the experimental data may reflect an uncomplete relaxation of the lattice mismatch between the GaN buffer layer and the InN film, given the much higher value of C_{33} observed in single crystalline GaN. Note that the uppermost monolayers contribute more to the IXS signal than the lower ones, due to attenuation of both incident and scattered x-rays. Despite probing only the upper 2 micron film layer, strain effects seem to influence the observed mechanical behavior.

Figure 3 displays the phonon dispersion relations determined in InN corresponding to the energy range of quasi-acoustic branches, which are dominated by atomic displacements of the Indium sublattice. Different symbols are used to plot IXS data originating from different scattering polarization geometries. Both GGA and LDA approximations yield phonon frequencies (solid curves) in excellent agreement with the experimental data (symbols). We were able to determine the value at the Γ point, 230(1) cm^{-1}, and the dispersion of the lower energy silent B_1 mode, which appears frequently in Raman spectra of doped nitrides due to the induced lattice disorder[22]. Most of the data (blue solid circles) were taken using an in-plane scattering geometry with mixed longitudinal and transverse character, taking full advantage of the multi-analyzer spectrometer of ID28. The (red) squares display data obtained with an IXS scattering geometry involving modes polarized along the c-axis, whereas the dashed curves display the calculated phonon branches with eigenvectors at the Γ point

6

polarized along the same axis. There is excellent agreement between experimental and calculated data. Raman data for the lower energy E_2 mode, 87 cm^{-1}, reported by Davydov and coworkers[6] are also in agreement with the extrapolation of IXS data at low momentum transfers, 90(1) cm^{-1}. Issues related with the sample alignment restricted the experiment to measure the lower energy phonon branches, though the technique is also suitable for probing higher energy branches.

In conclusion, this work demonstrates the feasibility of grazing incidence IXS to provide thorough information on the lattice dynamics of thin films, with interest in many fields of material science, such as novel advanced materials, semiconductors and superconductors. We have discussed results on the quasi-acoustic phonon dispersion relations and the elastic stiffness tensor of a thin film of InN. The five independent components of the elastic stiffness tensor have been obtained in a self-consistent manner and compared with calculations performed using first-principles methods. Phonon frequencies and polarizations have been determined for the 6 lower energy branches of the InN phonon dispersion relations, providing useful information about the energy and dispersion of the silent B_1 mode at 230 cm $^{-1}$. The experimental data have been analyzed with the aid of *ab initio* calculations. The calculated phonon frequencies, polarizations, and elastic constants display an excellent agreement with the experimental data. We hope that this work will stimulate further experimental studies of phonon dispersion relations and elastic constants in thin films.

———————

* jserrano@fa.upc.edu

[1] J. Wu, W. Walukiewicz, K. Yu, J. Ager, E. Haller, H. Lu, W. Schaft, Y. Saito, and Y. Nanishi,

Appl. Phys. Lett. (2002).

2 V. Y. Davydov, A. A. Klochikhin, R. P. Seisyan, V. V. Emtsev, S. V. Ivanov, F. Bechstedt, J. Furthmüller, H. Harima, A. V. Mudryi, J. Aderhold, et al., phys. stat. sol. (b) **229**, R1 (2002).

3 R. Jones, K. Yu, S. Li, W. Walukiewicz, J. Ager, E. Haller, H. Lu, and W. Schaff, Phys. Rev. Lett. **96**, 125505 (2006).

4 J.-H. Song, T. Akiyama, and A. Freeman, Phys. Rev. Lett. **101**, 186801 (2008).

5 Z. Qian, W. Shen, H. Ogawa, and Q. Guo, J. Phys.: Condens. Matter **16**, R381 (2004).

6 V. Y. Davydov, V. V. Emtsev, N. Goncharuk, A. N. Smirnov, V. D. Petrikov, V. V. Mamutin, V. A. Vekshin, and S. V. Ivanov, Appl. Phys. Lett. **75**, 3297 (1999).

7 B. M. Murphy, H. Requardt, J. Stettner, J. Serrano, M. Krisch, M. Müller, and W. Press, Phys. Rev. Lett. **95**, 256104 (2005).

8 A. Majumdar, ASME J. Heat Transfer **115**, 7 (1993).

9 K. Xu and A. Yoshikawa, Appl. Phys. Lett. **83**, 251 (2003).

10 H. Reichert, F. Bencivenga, B. Wehinger, M. Krisch, F. Sette, and H. Dosch, Phys. Rev. Lett. **98**, 096104 (2007).

11 X. Gonze, J.-M. Beuken, R. Caracas, F. Detraux, M. Fuchs, G.-M. Rignanese, L. Sindic, M. Verstraete, G. Zerah, F. Jollet, et al., Comput. Mat. Sci. **25**, 478 (2002).

12 X. Gonze, G.-M. Rignanese, M. Verstraete, Y. P. J.-M. Beuken, R. Caracas, F. Jollet, M. Torrent, G. Zerah, M. Mi-kami, P. Ghosez, et al., Z. Kristallogr. **220**, 558 (2005).

13 X. Gonze, B. Amadon, P.-M. Anglade, J.-M. Beuken, F. Bottin, P. Boulanger, F. Bruneval, D. Caliste, R. Caracas, M. Cote, et al., Computer Phys. Comm. **180**, 2582 (2009).

14 N. Troullier and J. L. Martins, Phys. Rev. B **43**, 1993 (1991).

15 C. Hartwigsen, S. Goedecker, and J. Hutter, Phys. Rev. B **58**, 3641 (1998).

16 K. Sarasamak, S. Limpijumnong, and W. Lambrecht, Phys. Rev. B **82**, 035201 (2010).

17 B. A. Auld, *Acoustic Fields and Waves in Solids, vol. I and II* (Krieger Publishing, Malabar, 1990), 2nd ed.

18 A. Sheleg and V. Savastenko, Izv. Akad. Nauk. SSSR, Neorg. Mater. **15**, 1598 (1979).

19 K. Kim, W. R. L. Lambrecht, and B. Segall, Phys. Rev. B **53**, 16310 (1996).

20 A. Wright, J. Appl. Phys. **82**, 2833 (1997).

21 S. P. Lepkowski, J. A. Majewski, and G. Jurczak, Phys. Rev. B **72**, 245201 (2005).

TABLE I: Summary of investigated acoustic phonon branches to obtain the elastic stiffness tensor. We indicate the direction of the total momentum transfer, the phonon propagation and polarization vectors and the apparent sound velocity obtained from the fit of the dispersion with a sinusoidal function. The parameter ξ is always positive.

Notation	Momentum transfer	Propagating vector	Polarization vector	Velocity (km/s)
LA[100]	[2+ξ 0 0]	[1 0 0]	$\langle 100 \rangle$	5.70(9)
LA[001]	[0 0 2+ξ]	[0 0 1]	$\langle 001 \rangle$	6.18(3)
TA[010]$_{\langle 100 \rangle}$	[2 ξ 0]	[0 1 0]	$\langle 100 \rangle$	2.29(18)
TA[100]$_{\langle 001 \rangle}$	[ξ 0 2]	[1 0 0]	$\langle 001 \rangle$	2.81(8)
LA[203]	[2+ξ 0 3+ξ]	[2 0 3]	$\langle 203 \rangle$	3.11(10)

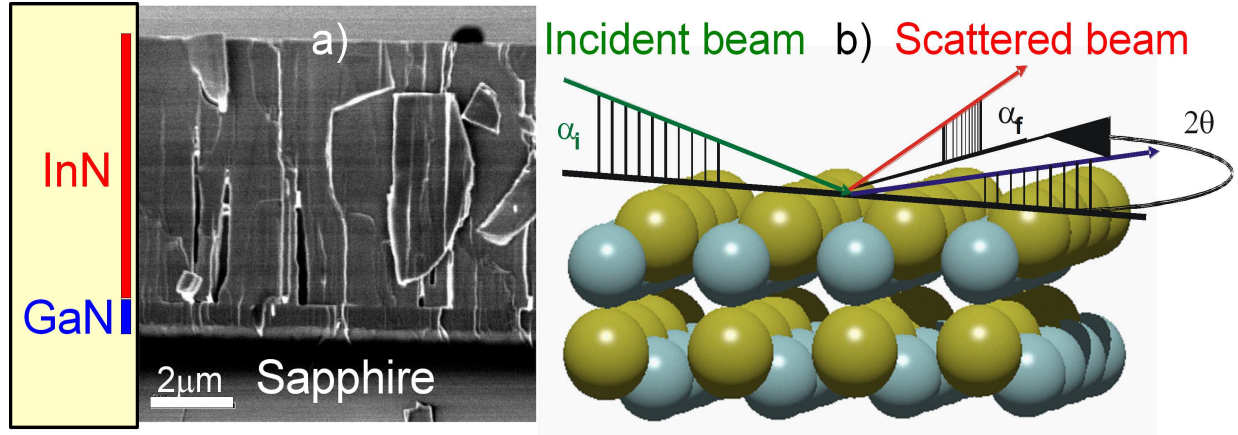[22] F. J. Manjón, B. Marí, J. Serrano, and A. H. Romero, J. Appl. Phys. **97**, 053516 (2005).

FIG. 1: (Color online) (a) SEM image of the wurtzite InN film. The horizontal bar displays a length of 2μm. (b) Grazing incidence IXS geometry, where α_i and α_f are 1.7 degrees. The 2θ angle determines the total momentum transfer selected by the spectrometer.

TABLE II: Elastic stiffness tensor obtained by IXS, other experimental data, and *ab initio* calculations, in GPa. For completeness, we include the values for the bulk modulus, B, and the biaxial elastic modulus, $G_{ab} = C_{11} + C_{12} - 2C_{13}^2/C_{33}$.

	IXS	Other exp.	*ab-initio*		Other calc.
			LDA	GGA	
C_{11}	**225(7)**	$190(7)^1$	224	238	271^2, 232^3, 223^4, 229^5
C_{12}	**152(13)**	$104(3)^1$	112	112	124^2, 115^3, 115^4, 120^5
C_{13}	**109(7)**	$121(7)^1$	91	92	94^2, 96^3, 92^4, 95^5
C_{33}	**265(3)**	$182(6)^1$	243	237	200^2, 239^3, 224^4, 234^5
C_{44}	**55(3)**	$10(1)^1$	46	57	46^2, 52^3, 48^4, 49^5
C_{66}	**37(6)**	$43(5)^1$	56	63	74^2, 59^3, 54^4, 55^5
B_0	162	139^1	142	145	147^2, 151^3, 141^4, 146^5
G_{ab}	287	133^1	268	279	307^2, 270^3, 262^4, 271^5

[1] Temperature-dependent x-ray broadening, Ref.18

[2] LDA, Full-potential linear-muffin-tin-orbitals (FP-LMTO) and tensor transformations, Ref.19

[3] LDA, FP-LMTO, Ref.16

[4] LDA, plane wave pseudopotentials, Ref.20

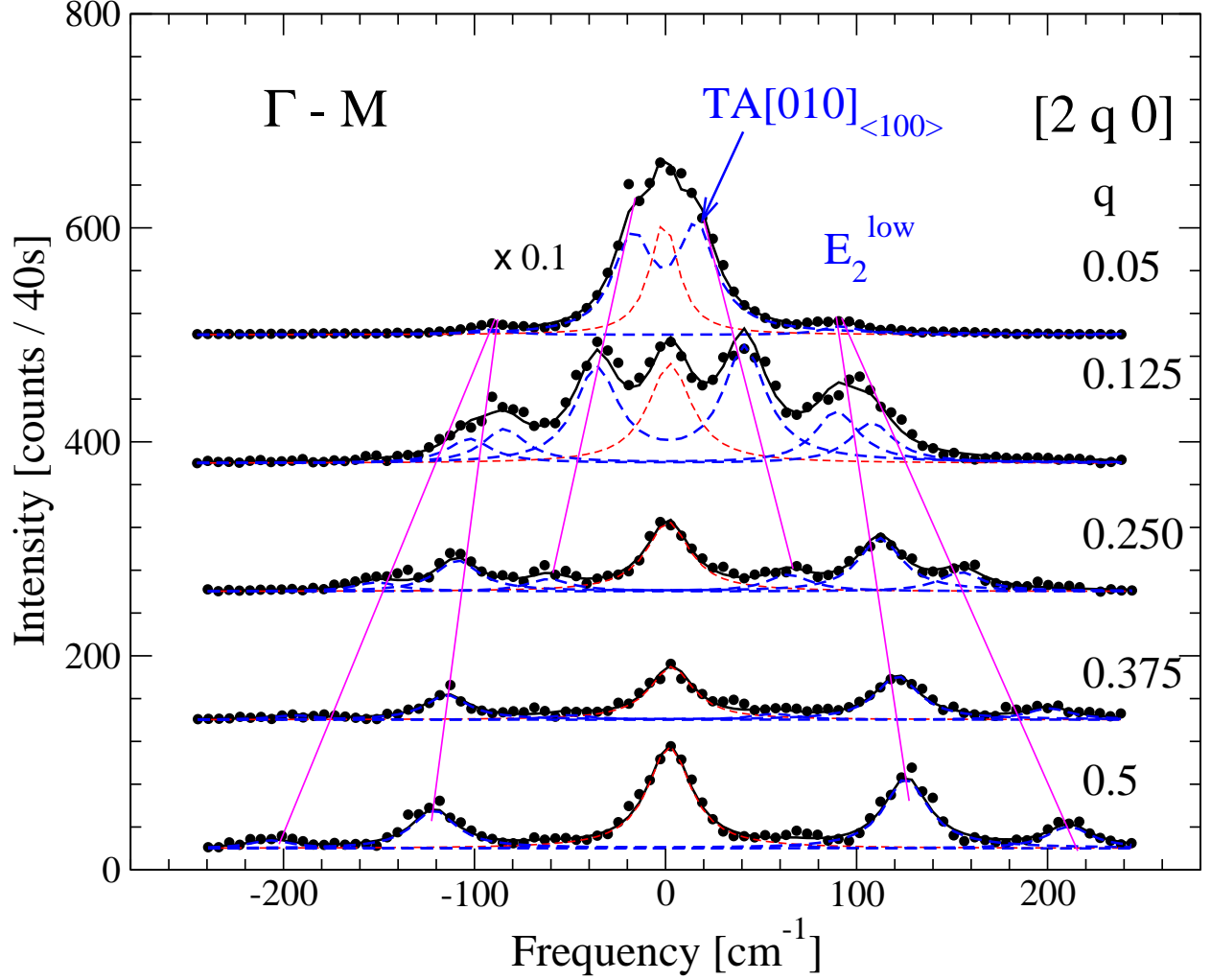[5] LDA, plane wave pseudopotentials, Ref.21

FIG. 2: (Color online) Selected IXS spectra corresponding to transverse quasi-acoustic modes for momentum transfer values along the $\Gamma - M$ direction of the BZ. The symbols display the experimental data whereas the solid curves represent the best fit to the spectra. Dashed lines are used to indicate the contributions of different excitations (blue) and the zero-energy central elastic peak (red). The nearly vertical lines are guides-to-the-eye to highlight the different phonon branch dispersions with increasing momentum transfer. The $\xi = 0.05$ spectrum intensity has been multiplied by a factor 0.1 to better display the mode dispersion. Note the drastic decrease in TA intensity with increasing momentum transfer.
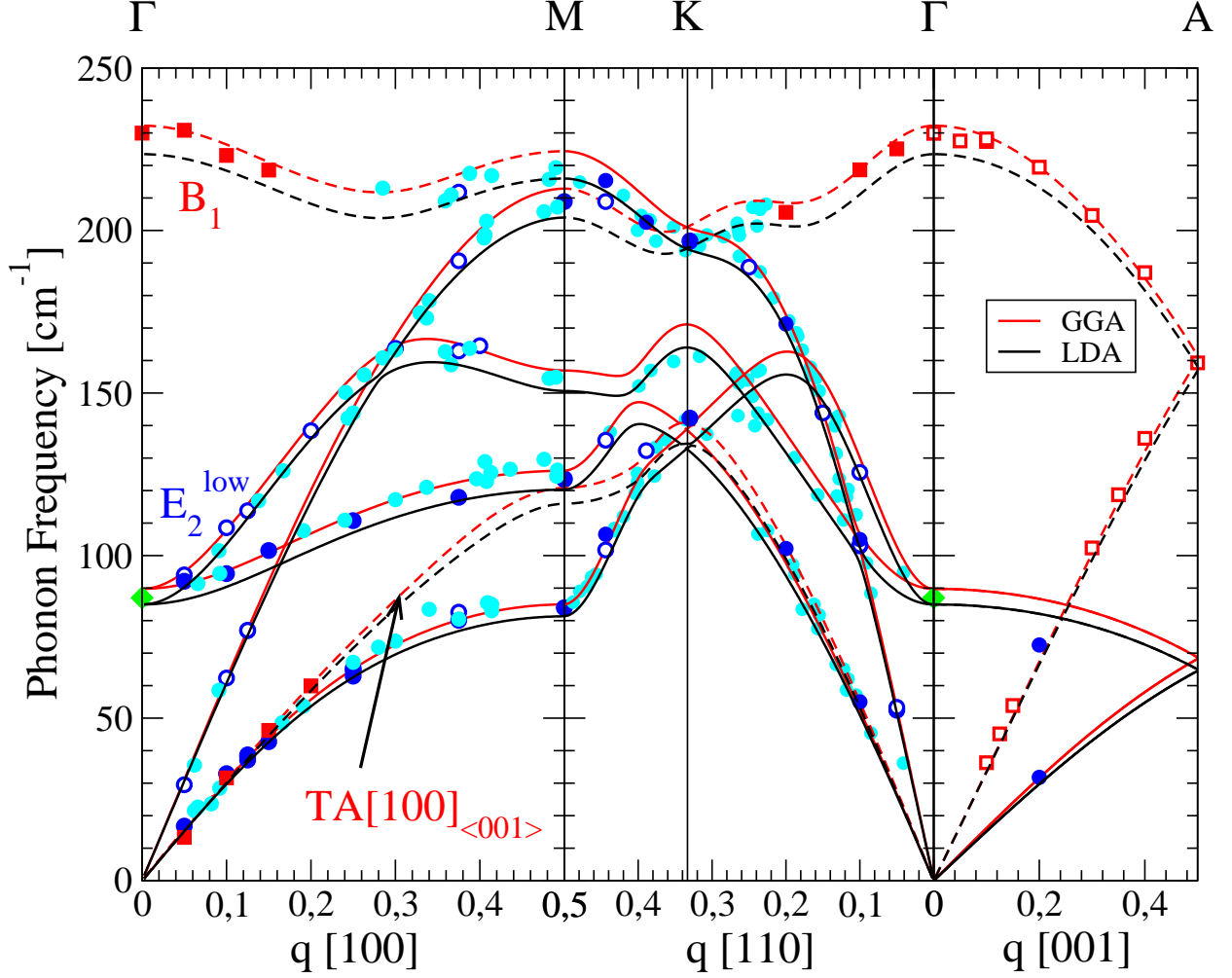
FIG. 3: (Color online) Quasi-acoustic phonon dispersion relations of wurtzite InN along the main symmetry directions. Open and solid simbols display IXS data corresponding to longitudinal and transverse modes, respectively, except for the solid cyan circles that display IXS data obtained using mixed transverse and longitudinal polarizations. The black (red) curves plot results obtained from LDA (GGA) *ab initio* calculations. Modes polarized along the ⟨001⟩ direction of the BZ are represented by (red) squares and dashed lines, whereas in-plane polarized modes are represented by (blue) circles and solid lines. The green diamond at the Γ point shows Raman data for the E_2^{low} mode from Ref.6. Momentum transfers in the x-axes are given in reciprocal lattice units.